Journal of the Optical Society of America B
OPTICAL PHYSICS

Efficient nonlinear metasurfaces by using multiresonant high-Q plasmonic arrays

Mikko J. Huttunen,[1,*] Orad Reshef,[2] Timo Stolt,[1] Ksenia Dolgaleva,[2,3] Robert W. Boyd,[2,3,4] and Martti Kauranen[1]

[1]Photonics Laboratory, Physics Unit, Tampere University, P.O. Box 692, FI-33014 Tampere, Finland
[2]Department of Physics, University of Ottawa, Ottawa, Ontario K1N 6N5, Canada
[3]School of Electrical Engineering and Computer Science, University of Ottawa, Ottawa, Ontario K1N 6N5, Canada
[4]The Institute of Optics and Department of Physics and Astronomy, University of Rochester, Rochester, New York 14627, USA
*Corresponding author: mikko.huttunen@tuni.fi

Received 30 January 2019; revised 21 March 2019; accepted 24 March 2019; posted 25 March 2019 (Doc. ID 359213); published 25 April 2019

We numerically investigate second-harmonic generation from multiresonant plasmonic metasurfaces by designing an array consisting of L-shaped aluminum nanoparticles that simultaneously supports two surface lattice resonances with relatively high quality factors (>100). Using an approach based on the nonlinear discrete-dipole approximation, we predict an over million-fold enhancement of the emitted second-harmonic intensity from a particle at the center of the metasurface compared to an individual particle and estimate that conversion efficiencies of around 10^{-5} could be achievable from the surface. Our results are an important step towards making nonlinear metasurfaces practical for nonlinear applications, such as for frequency conversion.

https://doi.org/10.1364/JOSAB.36.000E30

1. INTRODUCTION

Nonlinear optical processes are important in many diverse fields ranging from biomedical imaging to ultrafast spectroscopy [1–3]. An everyday challenge of nonlinear optics is that intrinsic material nonlinearities are very weak. Consequently, intense pulsed laser sources and bulky nonlinear materials such as crystals or fibers are commonly used to enable efficient nonlinear processes [4]. Due to recent progress in nanophotonics and metamaterials, there is a growing demand for smaller and more efficient nonlinear optical components. However, this miniaturization task is very challenging to accomplish by using traditional materials, which motivates the search for alternative approaches.

Recently, plasmonic metamaterials have emerged as viable candidates for efficient nanoscale nonlinear optics [5]. Metal nanoparticles support collective oscillations of conduction electrons, known as localized surface plasmons (LSPs), which can enhance the local field near the nanoparticles considerably [6]. This local-field enhancement is especially important for nonlinear interactions, because nonlinear optical processes scale with higher powers of the local field. Interestingly, at resonant conditions, local fields can be even further enhanced, a fact that has also been utilized in many applications ranging from surface-enhanced Raman spectroscopy to near-field scanning microscopy [7–9]. Very recently, multiresonant structures have been studied due to their potential for boosting nonlinear processes [10–14]. In these structures, both input and signal fields of nonlinear origin are enhanced due to simultaneously occurring multiple resonances.

Despite steady progress, multiresonant structures have yet to be exploited to demonstrate dramatically more efficient nonlinear metamaterials. This is mostly because metasurface designs depend on LSP resonances, which are associated with low quality factors ($Q < 10$). However, relatively high-Q-factor resonances ($Q > 100$) can be achieved by arranging metal nanoparticles into periodic arrays, where particles become optically coupled and give rise to very narrow resonances, known as surface lattice resonances (SLRs) [15–18]. In fact, SLRs have already been utilized in many applications [19–22], where several works have also investigated their potential for nonlinear optics [23–29]. However, the nonlinear responses of multiresonant and high-Q-factor SLR arrays have not yet been investigated.

In this paper, we numerically investigate second-harmonic generation (SHG) from doubly resonant metasurfaces consisting of arrays of L-shaped aluminum nanoparticles. We use full-wave numerical simulations and the nonlinear discrete-dipole approximation (NDDA) approach to design a doubly resonant metasurface, calculate Q-factor values of the associated resonance peaks, perform SHG simulations, and estimate achievable conversion efficiencies. We predict an over six orders-of-magnitude enhancement of SHG emission from a particle at the center of

the array compared to a single particle. We also estimate that conversion efficiencies around 10^{-5} could be easily reachable using such metasurfaces.

2. THEORY

We use the NDDA approach to understand how multiresonant metasurfaces can be realized by arranging nanoparticles into periodic arrays supporting SLRs. The treatment follows earlier work on utilizing SLRs in nonlinear optics [26–28].

We start by taking an applied field of the form $\mathbf{E}_{\text{inc}}(\omega) = \mathbf{E}_0 \exp(i\mathbf{k}\cdot\mathbf{r} - i\omega t)$, where $\mathbf{E}_0$ is the field amplitude, $\mathbf{k}$ is the wave vector, $\mathbf{r}$ is the position vector, ω is frequency, and t is time. This field is incident on a metasurface consisting of N nanoparticles, in which case the response of the jth particle at location $\mathbf{r}_j$ is also affected by scattered fields due to all other particles. The local field at the jth particle is then written as

$$\mathbf{E}_{\text{loc},j}(\omega) = \mathbf{E}_{\text{inc},j}(\omega) - \sum_{k\neq j}\mathbf{A}_{jk}(\omega)\mathbf{p}_k(\omega), \tag{1}$$

where $\mathbf{A}_{jk}(\omega)$ is a 3×3 matrix describing the interaction between jth and kth particles at frequency ω. For small nanoparticles surrounded by a homogeneous medium, this interaction term is given by [18,30]

$$\mathbf{A}_{jk}(\omega) = \frac{e^{ikr_{jk}}}{\epsilon_0 r_{jk}}\left[k^2(\hat{\mathbf{r}}_{jk}\hat{\mathbf{r}}_{jk}^{\mathsf{T}} - \mathbf{I}) - \frac{1-ikr_{jk}}{r_{jk}^2}(3\hat{\mathbf{r}}_{jk}\hat{\mathbf{r}}_{jk}^{\mathsf{T}} - \mathbf{I})\right], \tag{2}$$

where ϵ_0 is the vacuum permittivity, $k = n\omega/c = 2\pi n/\lambda$ is the wavenumber, c is the speed of light in vacuum, λ is wavelength, n is the refractive index of the surrounding medium, r_{jk} is the distance between the dipoles, $\hat{\mathbf{r}}_{jk}$ and $\hat{\mathbf{r}}_{jk}^{\mathsf{T}}$ are the unit vector pointing in the direction from $\mathbf{r}_j$ to $\mathbf{r}_k$ along with its transpose, respectively, and terms $\mathbf{I}$ are 3×3 identity matrices. This interaction term should be modified when particles associated with multipolar emission patterns are investigated, as was noted in Ref. [26].

The dipole moment of the jth particle is defined as

$$\mathbf{p}_j(\omega) = \epsilon_0\alpha(\omega)\mathbf{E}_{\text{loc},j}(\omega). \tag{3}$$

Here we assume that the polarizability of the particle is given by [17,31]

$$\alpha(\omega) = \frac{\alpha_{\text{static}}(\omega)}{1 - \frac{2}{3}ik^3\alpha_{\text{static}}(\omega) - \frac{k^2}{l}\alpha_{\text{static}}(\omega)}, \tag{4}$$

where l is the effective length of the particle. The term α_{static} is a static polarizability of a small nanoparticle and is written as

$$\alpha_{\text{static}}(\omega) = \frac{A_0}{(\omega_{\text{res}} - \omega) + i\gamma}, \tag{5}$$

where A_0 is a constant, and ω_{res} and γ are related to the center frequency and the half-width of the LSP resonance, respectively. These parameters may be determined empirically (e.g., by curve fitting to numerical simulations). In essence, by using Eq. (4), the static polarizability α_{static} is modified to take into account the effects of radiative damping and dynamic depolarization, improving the accuracy of the approach, especially at longer wavelengths [31].

By adopting notation $\mathbf{A}_{jj}(\omega) = \epsilon_0^{-1}\alpha^{-1}(\omega)$, we can now rewrite Eq. (1) as a system of $3N$ linear equations given by

$$\mathbf{E}_{\text{inc},j}(\omega) = \sum_{k=1}^{N}\mathbf{A}_{jk}(\omega)\mathbf{p}_k(\omega), \tag{6}$$

which can be combined with Eq. (3) to solve for the local field $\mathbf{E}_{\text{loc}}$ [18,32]. Looking at the above equations, we see that $\mathbf{E}_{\text{loc}}$ and $\mathbf{p}$ are both affected by the scattered fields. Interestingly, this effect can considerably modify the linear optical responses of metasurfaces [16,17,21,22].

The final step is to extend the above approach to the nonlinear process of SHG. A more general case has been considered earlier with a focus on singly resonant metasurfaces [27]. We assume that the undepleted-pump approximation holds, allowing us to write the SHG dipole moment component for the jth particle as

$$\mathbf{p}_{\text{exc},j}(2\omega) = \epsilon_0\beta(2\omega;\omega,\omega):\mathbf{E}_{\text{loc},j}(\omega)\mathbf{E}_{\text{loc},j}(\omega), \tag{7}$$

where β is the first hyperpolarizability tensor. Next, we need to include contributions of the scattered fields from all other dipoles on the jth dipole moment $\mathbf{p}_j(2\omega)$. This is done by forming and solving another system of $3N$ linear equations written as

$$\epsilon_0^{-1}\alpha^{-1}(2\omega)\mathbf{p}_{\text{exc},j}(2\omega) = \sum_{k=1}^{N}\mathbf{A}_{jk}(2\omega)\mathbf{p}_k(2\omega). \tag{8}$$

The SHG response of a metasurface can now be predicted with the aid of the above equations [27,28]. Specifically, the form of Eq. (8) gives rise to an additional lattice resonance contribution to the SHG response, facilitating the design of doubly resonant metasurfaces. A nice demonstration of the existence and possibility to use this contribution for enhancing SHG responses has been recently given in Ref. [26].

3. DESIGN FOR DOUBLY RESONANT METASURFACE

Next we design a doubly resonant metasurface that simultaneously supports a high-Q-factor SLR at the pump frequency ω (SLR_ω) and at the SHG frequency 2ω ($\text{SLR}_{2\omega}$). We consider a rectangular array and a situation where the two SLRs oscillate along perpendicular lattice directions [see Fig. 1(a)]. Particularly, we arrange the SLR_ω ($\text{SLR}_{2\omega}$) to arise due to inter-particle coupling in the y direction (x direction). This way, changes in the lattice period along x (y) do not markedly affect the $\text{SLR}_{2\omega}$ (SLR_ω) center frequency, simplifying the design process. We note that by utilizing coupling along diagonal lattice directions, one could also design triply resonant metasurfaces for non-degenerate processes such as sum-frequency generation or difference-frequency generation [18,27].

In our lattice configuration, the local field at the pump frequency $\mathbf{E}_{\text{loc}}(\omega)$ is enhanced due to strong lattice coupling between particles along the y direction [see Fig. 1(a)]. Consequently, nanoparticles should exhibit polarizability with a strong x component $\alpha_x(\omega)$. In this case, particles will efficiently scatter incident x-polarized light along y direction, giving rise to SLR_ω [18]. Similarly, when we enhance the local

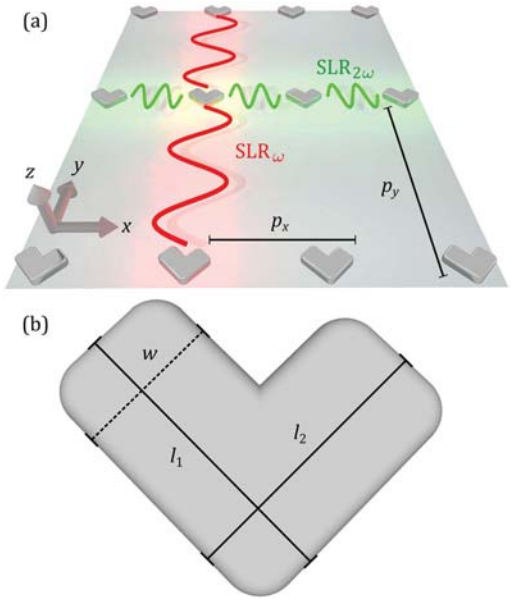

Fig. 1. (a) Multiresonant metasurface consisting of periodically arranged L-shaped aluminum nanoparticles. By adjusting periods $p_x \approx \lambda_{fun}/n$ and $p_y \approx \lambda_{SHG}/n$, two high-$Q$-factor SLRs can be designed to simultaneously peak at the fundamental and SHG wavelengths. (b) Schematic for an individual asymmetric L-shaped nanoparticle with thickness h, left-side (right-side) arm length l_1 (l_2) and arm width w.

field at the SHG frequency $\mathbf{E}_{loc}(2\omega)$, we need strong lattice coupling along x, and therefore $\alpha_y(2\omega)$ should be strong.

The two above conditions are seemingly easily fulfilled, for example, by using rectangular nanoparticles [33]. However, complications arise because SHG is a second-order nonlinear process and is therefore strongly affected by symmetry considerations [4]. In particular, centrosymmetric structures, such as rectangular nanoparticles, do not exhibit SHG responses that are allowed under electric dipole approximation when illuminated with a plane wave at normal incidence [34]. Therefore, nanoparticles with low symmetry should be used. Here, we investigated asymmetric L-shaped nanoparticles with two unequal arms of lengths l_1 and l_2 [see Fig. 1(b)], possessing a hyperpolarizability tensor with all components being nonzero. In this work, we were interested in the β_{yxx} component, because it facilitates coupling of the two orthogonally oscillating SLRs by allowing x-polarized fundamental field to give rise to a y-polarized SHG dipole moment [see Eq. (7)].

Next, we performed full-wave numerical simulations using finite-difference time domain (FDTD) software Lumerical FDTD Solutions in order to optimize the structure of the metasurface. The operating wavelength was chosen to be 1200 nm resulting in SHG emission at 600 nm, and the metasurface was assumed to be embedded in a homogeneous medium with $n = 1.51$. In order to realize SLRs with high Q-factors, scattering and absorption losses of the metasurface should be minimized. To minimize absorption losses related to LSP resonances, small nanoparticles should be used. However, small nanoparticles scatter light only weakly, resulting in weak SLRs [18]. Here, we decided to use asymmetric L-shaped aluminum nanoparticles with thickness $h = 30$ nm, left-side arm length $l_1 = 100$ nm, right-side arm length $l_2 = 90$ nm, and arm width $w = 45$ nm [see Fig. 1(b)]. Sharp corners of the particles were rounded with the radius of 10 nm. The particles were chosen to be made of aluminum instead of gold, which is typically used in plasmonic applications. This material choice allowed the shorter wavelength LSP resonance to occur near 470 nm, which resulted in high-Q SLRs. These particles were arranged into a rectangular lattice with the periods $p_x = 395$ nm and $p_y = 793$ nm, giving rise to the two high-Q SLRs at the SHG and the fundamental wavelengths, respectively.

4. RESULTS AND DISCUSSION

We performed FDTD simulations to investigate the linear optical responses of both individual L-shaped nanoparticles and their arrays. We used the total-field scattered-field method to simulate transmission spectra of individual particles for x- and y-polarized incident light at normal incidence [see Fig. 2(a)]. The simulated transmission spectra verified that incident x-polarized (y-polarized) light is optimally coupled to plasmon oscillations related to the longer (shorter) wavelength LSPR of the L-shaped nanoparticles [35]. Metasurface simulations were performed by using periodic boundary conditions, and the simulation time was set to 4 ps. Simulated transmission spectra for x- and y-polarized incident light at normal incidence are shown in Fig. 2(b). The peak wavelength of the occurring shorter (longer) wavelength LSP resonance was found to be

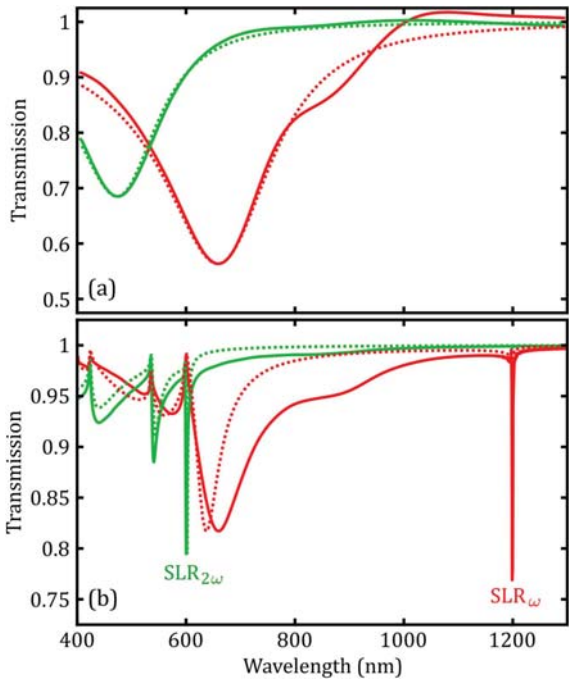

Fig. 2. Transmission spectra of (a) individual L-shaped aluminum nanoparticles and (b) nanoparticle arrays. Green (red) lines correspond to y-polarized (x-polarized) incident light. Solid (dotted) lines correspond to FDTD (DDA) simulations, where DDA spectra have been scaled so that the peaks around 600 nm are equally strong. The main discrepancy between FDTD and DDA simulations near 800 nm is due to interband transitions of aluminum, which were neglected in the DDA simulations.

472 nm (657 nm) [see Fig. 2(a)], and $SLR_{2\omega}$ (SLR_{ω}) was verified to peak close to 600 nm (1200 nm) [see Fig. 2(b)]. By estimating the full-width at half maximum values of the SLR peaks, we calculated the associated Q-factors to be around 250 and 800 for $SLR_{2\omega}$ and SLR_{ω}, respectively.

We then performed linear and SHG simulations by using the above-mentioned NDDA method [27,28]. The simulated metasurface consisted of 600 × 600 particles corresponding to a physical size of around 250 × 500 μm^2, and was illuminated by a normally incident x-polarized plane wave. Polarizability components $\alpha_x(\omega)$ and $\alpha_y(2\omega)$ were found by curve fitting two transmission line profiles simulated using the NDDA method to the respective spectra simulated by using the FDTD method [see Fig. 2(a)]. Parameters resulting in a good fit were found to be $A_0^x = 0.48$ cm^3 s^{-1}, $A_0^y = 0.24$ cm^3 s^{-1}, $\omega_{\text{res}}^x = 4.0 \times 10^{15}$ s^{-1}, $\omega_{\text{res}}^y = 5.2 \times 10^{15}$ s^{-1}, and $\gamma = 7.96 \times 10^{13}$ s^{-1}. Simulated transmission spectra of the metasurface using the NDDA method (dotted lines) are shown in Fig. 2(b), which agree quite well with the full-wave FDTD simulations (solid lines). As expected, the only relevant non-zero hyperpolarizability tensor component was found to be β_{yxx}.

The simulated SHG emission enhancement for one particle at the center of the metasurface is shown in Fig. 3, where over million-fold (1,389,200-fold) enhancement in the SHG emission intensity occurs for the fundamental field at 1200 nm (black solid line in Fig. 3). The result is scaled with respect to SHG emission from a single isolated nanoparticle. In order to verify that the enhancement was of doubly resonant origin, we repeated SHG simulations while slightly varying the period p_x. Variations in p_x affect the position of $SLR_{2\omega}$ and make the metasurface singly resonant. The slight detuning of the period from the value $p_x = 395$ nm to 393 nm and 398 nm resulted in one to two orders of magnitude decrease in the overall SHG enhancement at 1200 nm (see respective red and blue dotted lines in Fig. 3). Particularly, the simulated SHG enhancement factors were found to be 465,900 and 31,600 for $p_x = 393$ nm and 398 nm, respectively. It is clear by looking at these values that most of the resonance enhancement predicted for the doubly resonant metasurface occurs due to resonance enhancement at the fundamental wavelength. However, this is expected because the SHG process depends quadratically on the fundamental field strength. In addition to the expected decrease in SHG enhancement at 1200 nm, new resonance peaks appeared on the SHG spectra (highlighted with arrows). These results verified the doubly resonant origin of the original SHG enhancement using $p_x = 395$ nm.

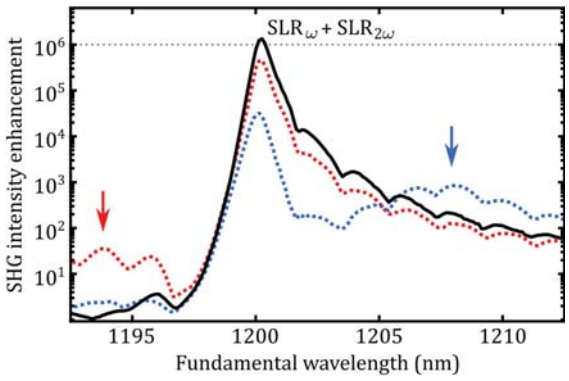

Fig. 3. Predicted SHG emission intensity enhancement for a single particle at the center of the metasurface. Over million-fold (1,389,200-fold) enhancement of SHG emission occurs for the doubly resonant metasurface (black solid line), in comparison to a single particle. The doubly resonant origin of the enhancement is verified by varying p_x, which results in decreased SHG emission near 1200 nm (red and blue dotted lines). The red (blue) dotted line corresponds to $p_x = 393$ nm (398 nm). The simulated SHG enhancement factors were found to be 465,900 and 31,600 for $p_x = 393$ nm and 398 nm, respectively. The features appearing in the spectra due to the de-tuned $SLR_{2\omega}$ are highlighted with arrows.

Next, we provide an order-of-magnitude estimate for SHG conversion efficiency that could be reached using the designed metasurface. Because quantitative SHG responses from aluminum nanoparticles have not been reported so far, our estimates are based on similar gold nanoparticles. In our previous study [28], we estimated the SHG conversion efficiency of an array of L-shaped gold nanoparticles to be 6×10^{-12}. In this study, the excitation of the nanoparticles was non-resonant, and was performed by an unamplified fs-laser with modest peak intensity of around 60 MW/cm^2 at the sample plane. Therefore, we estimate SHG conversion efficiencies around 10^{-5} to be easily reachable with the proposed doubly resonant metasurfaces using a single-pass configuration and pumping conditions similar to the ones used in the previous study. Higher conversion efficiencies are likely to be achievable either by utilizing multi-pass pumping schemes or by designing metasurfaces able to withstand more intense pumping conditions [36]. For example, single-pass non-multiresonant metasurfaces have already reported high third-harmonic generation conversion efficiencies (0.45%) [37]. By applying the approach introduced here, conversion efficiencies would be increased to a level that may truly begin to be useful for practical frequency conversion applications. Although the estimated conversion efficiency is not yet comparable to what is achieved using traditional nonlinear materials, such as crystals, the studied metasurface with thickness of 30 nm is extremely thin, being advantageous for frequency conversion applications. For example, thin metasurfaces are free of phase-matching issues, which is important when dealing with traditional nonlinear materials [4].

We then compare the predicted SHG enhancement factors with earlier experimental work. The highest singly resonant SHG enhancement factor, reported to date, is 450 [29], which is two to three orders of magnitude lower than predicted here for the singly resonant case. It is often true that the theoretical and numerical predictions exceed the experimental values. However, we believe that this discrepancy between the performed experiments and the numerical predictions based on a widely accepted approach implies that experiments have not yet been performed on entirely optimized metasurfaces. In particular, the experimentally demonstrated Q-factors remain much lower than the ones we predict in the present paper.

Finally, we note that our approach is very general and could be used to enhance light–matter interactions in various nonlinear metasurfaces and metamaterials. Here, we restricted our study to SHG from L-shaped aluminum nanoparticles, but the approach could work also with other materials and particle

shapes of proper symmetry, such as split-ring resonators or related inverse Babinet structures [38]. In fact, the approach might be even more useful for enhancing nonlinear responses of dielectric metasurfaces [39], because such structures should be able to support resonances with considerably higher Q-factors than what is currently achievable with SLRs. In addition, it should be possible to combine this concept with recently introduced multiresonant nanostructures, where the nonlinear optical responses of individual nanoparticles already exhibit doubly resonant behavior [10,14].

5. CONCLUSION

We have demonstrated an approach to realize multiresonant metasurfaces, which could enable nonlinear optical applications such as frequency conversion. We have designed a metasurface consisting of L-shaped aluminum nanoparticles that simultaneously supports two surface lattice resonances with relatively high Q factors, and have numerically investigated second-harmonic emission from the metasurface. An over million-fold enhancement of the second-harmonic emission intensity is predicted, and power conversion efficiencies of around 10^{-5} are estimated to be reachable already using a single-pass configuration and modest pumping conditions. Because the approach is not restricted to any particular nanoparticle shape or material, it could provide a very general way to enhance optical nonlinearities of metamaterials for a variety of other nonlinear optical processes such as photon pair creation of THz-wave generation.

Funding. The Academy of Finland (265682, 287651, 308596, 320165); Natural Sciences and Engineering Research Council of Canada (NSERC).

Acknowledgment. M. J. H. and M. K. acknowledge the Flagship of Photonics Research and Innovation of the Academy of Finland. O. R. acknowledges the support of the Banting Postdoctoral Fellowship of the NSERC. K. D. acknowledges NSERC Discovery funding program. R. W. B. acknowledges support through the NSERC, the Canada Research Chairs program.

REFERENCES

1. T. Brabec and F. Krausz, "Intense few-cycle laser fields: frontiers of nonlinear optics," Rev. Mod. Phys. **72**, 545–591 (2000).
2. W. R. Zipfel, R. M. Williams, and W. W. Webb, "Nonlinear magic: multiphoton microscopy in the biosciences," Nat. Biotechnol. **21**, 1369–1377 (2003).
3. E. Garmire, "Nonlinear optics in daily life," Opt. Express **21**, 30532–30544 (2013).
4. R. W. Boyd, *Nonlinear Optics* (Academic, 2003).
5. M. Kauranen and A. V. Zayats, "Nonlinear plasmonics," Nat. Photonics **6**, 737–748 (2012).
6. S. A. Maier, *Plasmonics: Fundamentals and Applications* (Springer, 2007).
7. K. Kneipp, Y. Wang, H. Kneipp, L. T. Perelman, I. Itzkan, R. R. Dasari, and M. S. Feld, "Single molecule detection using surface-enhanced Raman scattering (SERS)," Phys. Rev. Lett. **78**, 1667–1670 (1997).
8. S. Rao, M. J. Huttunen, J. M. Kontio, J. Mäkitalo, M.-R. Viljanen, J. Simonen, M. Kauranen, and D. Petrov, "Tip-enhanced Raman scattering from bridged nanocones," Opt. Express **18**, 23790–23795 (2010).
9. H. Furukawa and S. Kawata, "Local field enhancement with an apertureless near-field-microscope probe," Opt. Commun. **148**, 221–224 (1998).
10. H. Aouani, M. Navarro-Cia, M. Rahmani, T. P. Sidiropoulos, M. Hong, R. F. Oulton, and S. A. Maier, "Multiresonant broadband optical antennas as efficient tunable nanosources of second harmonic light," Nano Lett. **12**, 4997–5002 (2012).
11. K. Thyagarajan, S. Rivier, A. Lovera, and O. J. Martin, "Enhanced second-harmonic generation from double resonant plasmonic antennae," Opt. Express **20**, 12860–12865 (2012).
12. K. Thyagarajan, J. Butet, and O. J. Martin, "Augmenting second harmonic generation using fano resonances in plasmonic systems," Nano Lett. **13**, 1847–1851 (2013).
13. M. Celebrano, X. Wu, M. Baselli, S. Großmann, P. Biagioni, A. Locatelli, C. De Angelis, G. Cerullo, R. Osellame, B. Hecht, L. Duò, F. Ciccacci, and M. Finazzi, "Mode matching in multiresonant plasmonic nanoantennas for enhanced second harmonic generation," Nat. Nanotechnol. **10**, 412–417 (2015).
14. K. Y. Yang, J. Butet, C. Yan, G. D. Bernasconi, and O. J. Martin, "Enhancement mechanisms of the second harmonic generation from double resonant aluminum nanostructures," ACS Photon. **4**, 1522–1530 (2017).
15. V. A. Markel, "Coupled-dipole approach to scattering of light from a one-dimensional periodic dipole structure," J. Mod. Opt. **40**, 2281–2291 (1993).
16. S. Zou, N. Janel, and G. C. Schatz, "Silver nanoparticle array structures that produce remarkably narrow plasmon lineshapes," J. Chem. Phys. **120**, 10871–10875 (2004).
17. B. Auguié and W. L. Barnes, "Collective resonances in gold nanoparticle arrays," Phys. Rev. Lett. **101**, 143902 (2008).
18. M. J. Huttunen, K. Dolgaleva, P. Törmä, and R. W. Boyd, "Ultra-strong polarization dependence of surface lattice resonances with out-of-plane plasmon oscillations," Opt. Express **24**, 28279–28289 (2016).
19. W. Zhou, M. Dridi, J. Y. Suh, C. H. Kim, D. T. Co, M. R. Wasielewski, G. C. Schatz, and T. W. Odom, "Lasing action in strongly coupled plasmonic nanocavity arrays," Nat. Nanotechnol. **8**, 506–511 (2013).
20. N. Meinzer, W. L. Barnes, and I. R. Hooper, "Plasmonic meta-atoms and metasurfaces," Nat. Photonics **8**, 889–898 (2014).
21. M. Kataja, T. K. Hakala, A. Julku, M. J. Huttunen, S. van Dijken, and P. Törmä, "Surface lattice resonances and magneto-optical response in magnetic nanoparticle arrays," Nat. Commun. **6**, 7072 (2015).
22. V. G. Kravets, A. V. Kabashin, W. L. Barnes, and A. N. Grigorenko, "Plasmonic surface lattice resonances: a review of properties and applications," Chem. Rev. **118**, 5912–5951 (2018).
23. R. Czaplicki, H. Husu, R. Siikanen, J. Mäkitalo, M. Kauranen, J. Laukkanen, J. Lehtolahti, and M. Kuittinen, "Enhancement of second-harmonic generation from metal nanoparticles by passive elements," Phys. Rev. Lett. **110**, 093902 (2013).
24. R. Czaplicki, J. Mäkitalo, R. Siikanen, H. Husu, J. Lehtolahti, M. Kuittinen, and M. Kauranen, "Second-harmonic generation from metal nanoparticles: resonance enhancement versus particle geometry," Nano Lett. **15**, 530–534 (2015).
25. R. Czaplicki, A. Kiviniemi, J. Laukkanen, J. Lehtolahti, M. Kuittinen, and M. Kauranen, "Surface lattice resonances in second harmonic generation from metasurfaces," Opt. Lett. **41**, 2684–2687 (2016).
26. L. Michaeli, S. Keren-Zur, O. Avayu, H. Suchowski, and T. Ellenbogen, "Nonlinear surface lattice resonance in plasmonic nanoparticle arrays," Phys. Rev. Lett. **118**, 243904 (2017).
27. M. J. Huttunen, P. Rasekh, R. W. Boyd, and K. Dolgaleva, "Using surface lattice resonances to engineer nonlinear optical processes in metal nanoparticle arrays," Phys. Rev. A **97**, 053817 (2018).
28. R. Czaplicki, A. Kiviniemi, M. J. Huttunen, X. Zang, T. Stolt, I. Vartiainen, J. Butet, M. Kuittinen, O. J. F. Martin, and M. Kauranen, "Less is more—enhancement of second-harmonic generation from metasurfaces by reduced nanoparticle density," Nano Lett. **18**, 7709–7714 (2018).
29. D. C. Hooper, C. Kuppe, D. Wang, W. Wang, J. Guan, T. W. Odom, and V. K. Valev, "Second harmonic spectroscopy of surface lattice resonances," Nano Lett. **19**, 165–172 (2018).
30. B. T. Draine and P. J. Flatau, "Discrete-dipole approximation for scattering calculations," J. Opt. Soc. Am. A **11**, 1491–1499 (1994).

31. T. Jensen, L. Kelly, A. Lazarides, and G. C. Schatz, "Electrodynamics of noble metal nanoparticles and nanoparticle clusters," J. Clust. Sci. **10**, 295–317 (1999).
32. M. A. Yurkin and A. G. Hoekstra, "The discrete dipole approximation: an overview and recent developments," J. Quant. Spectrosc. Radiat. Transf. **106**, 558–589 (2007).
33. B. Metzger, M. Hentschel, M. Lippitz, and H. Giessen, "Third-harmonic spectroscopy and modeling of the nonlinear response of plasmonic nanoantennas," Opt. Lett. **37**, 4741–4743 (2012).
34. R. Czaplicki, M. Zdanowicz, K. Koskinen, J. Laukkanen, M. Kuittinen, and M. Kauranen, "Dipole limit in second-harmonic generation from arrays of gold nanoparticles," Opt. Express **19**, 26866–26871 (2011).
35. H. Husu, J. Mäkitalo, J. Laukkanen, M. Kuittinen, and M. Kauranen, "Particle plasmon resonances in L-shaped gold nanoparticles," Opt. Express **18**, 16601–16606 (2010).
36. G. Albrecht, S. Kaiser, H. Giessen, and M. Hentschel, "Refractory plasmonics without refractory materials," Nano Lett. **17**, 6402–6408 (2017).
37. M. S. Nezami, D. Yoo, G. Hajisalem, S. H. Oh, and R. Gordon, "Gap plasmon enhanced metasurface third-harmonic generation in transmission geometry," ACS Photon. **3**, 1461–1467 (2016).
38. M. Hentschel, T. Weiss, S. Bagheri, and H. Giessen, "Babinet to the half: coupling of solid and inverse plasmonic structures," Nano Lett. **13**, 4428–4433 (2013).
39. Y. Kivshar, "All-dielectric meta-optics and non-linear nanophotonics," Natl. Sci. Rev. **5**, 144–158 (2018).